Non-linear control of a multi-string inverter configuration for a grid-connected photovoltaic system

Brahim Hameur[1,*], *Abdelmajid* Abouloifa[1], *Ibtissam* Lachkar[1], *Chaouqi* Aouadi[1], and *Abdelali* El Aroudi[2]

[1]ESE Laboratory, ENSEM, Hassan II University of Casablanca, Casablanca, Morocco
[2]Universitat Rovira i Virgili, Department of Electronics, Electrical Engineering and Automatic Control, Tarragona, Spain

Abstract. In this work, we have proposed to control and simulate a system composed of two DC-DC converters and a single DC-AC converter through several simulation scenarios. This configuration makes it possible to reduce the power processed by each converter and improve the system's flexibility. In this way, it becomes possible to control the number of panel strings to be operated according to the power required for grid injection. What's more, if some panels fail, the rest of the system continues to operate normally. This architecture also makes it possible to optimize maximum power point tracking (MPPT), particularly in the presence of partial shading. Simulation results show that the system remains stable, even under partial shading conditions and even if a panel ceases to operate.

1 Introduction

The systems for connecting photovoltaic panels to the electrical grid can be classified into different configurations: central inverter, string configuration (PV string), and multi-string configuration [1]. The central inverter configuration is generally used for high-power applications, typically between 500 kilowatts (kW) and 1 megawatt (MW) [2]. The PV string configuration uses several lower-power inverters (around 10 kW), allowing each string of panels to be controlled independently. These two configurations have only a single DC/AC conversion stage. In contrast, the multi-string configuration consists of two conversion stages: a DC/DC converter, which provides voltage boosting and maximum power point tracking (MPPT), and a DC/AC converter that injects the current into the grid. Unlike single-stage configurations, where the DC/AC converter is responsible for voltage boosting, MPPT tracking and DC-to-AC conversion, the separation of these functions in the multi-string configuration improves system flexibility, performance and reliability [3]. DC/DC converters used in photovoltaic systems are reviewed and analyzed in [4]. Among these converters is the boost converter, because in grid-connected systems the voltage of the photovoltaic panels is often lower than the voltage required at the inverter input. DC/AC converters are also presented in [5]. The most widely used conventional DC/AC converter is the two-level inverter. However, other types

*e-mail: brahim.hameur.doc22@ensem.ac.ma

of converters are also used, such as the H-Bridge Multilevel Inverter, the Flying Capacitor Inverter [6], and the NPC (Neutral Point Clamped) Multilevel Converter [7]. The main advantage of these converters over conventional three-phase two-level inverters is their ability to significantly reduce losses and to lower costs [8]. In this work, we design a control system for the proposed system, which consists of two boost-type DC/DC converters and a DC/AC converter (see Fig. 1), in order to evaluate its performance.

2 System Description and Modeling

2.1 System Description

The proposed system is composed of two boost-type DC/DC converters and a two-level voltage source converter (VSC) for DC/AC conversion, as illustrated in Fig. 1.

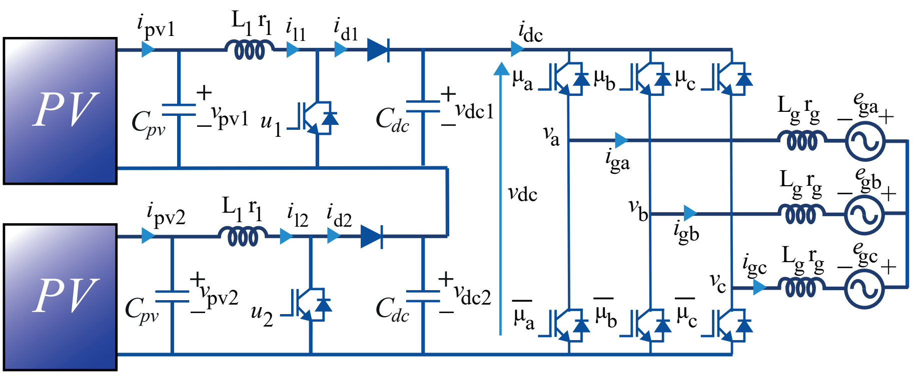

Figure 1. Schematic Diagram of the Grid-Connected PV System

2.2 The boost DC/DC converter model

To design the system controller, we must first present the mathematical model of these converters. By applying Kirchhoff's laws to the electrical circuit of the boost converter, we obtain its mathematical model(see Fig. 1).

$$C_{pv}\frac{dv_{pvj}}{dt} = i_{pvj} - i_{lj} \tag{1}$$

$$L_1\frac{di_{lj}}{dt} + r_1 i_{lj} = v_{pvj} - (1 - u_j)v_{dc1} \tag{2}$$

$$C_{dc}\frac{dv_{dcj}}{dt} = i_{dj} - i_{dc} \tag{3}$$

with j taking values 1 and 2. Boost converters use high-frequency switching devices that generate discontinuous signals. This discontinuous nature complicates the design of a direct control based on these signals. To overcome this difficulty, an averaged model is generally used. This model represents the average dynamic behavior of the converter over a switching period. with $(x_{1j}, x_{2j}, x_{3j}, x_{4j}, x_{5j}, x_6) = (< v_{pvj} >, < i_{lj} >, < i_{pvj} >, < i_{dj} >, < v_{dcj} >, <$

i_{dc} >) Thus, the mathematical model of the boost converter is represented by the following equations:

$$C_{pv}\frac{dx_{1j}}{dt} = x_{3j} - x_{2j} \tag{4}$$

$$L_1\frac{dx_{2j}}{dt} + r_1 x_{2j} = x_{1j} - (1 - u_j)x_{5j} \tag{5}$$

$$C_{dc}\frac{dx_{5j}}{dt} = x_{4j} - x_6 \tag{6}$$

2.3 DC/AC converter model

The DC/AC converter used in this system is a two-level converter. The mathematical model of this converter is given by :

$$L_2\frac{d(i_{gabc})}{dt} + r_2(i_{gabc}) = (v_{abc}) - (e_{gabc}) \tag{7}$$

$$(v_{abc}) = \frac{v_{dc}}{6}\begin{bmatrix} 2 & -1 & -1 \\ -1 & 2 & -1 \\ -1 & -1 & 2 \end{bmatrix}\begin{bmatrix} \mu_a \\ \mu_b \\ \mu_c \end{bmatrix} \tag{8}$$

By applying the Park transformation to equation (7), we obtain the model of the DC/AC converter in the dq0 reference frame.

$$L_2\frac{di_{gd}}{dt} + r_2 i_{gd} - L_2\omega i_{gq} = \mu_d\frac{v_{dc}}{2} - e_{gd} \tag{9}$$

$$L_2\frac{di_{gq}}{dt} + r_2 i_{gq} + L_2\omega i_{gd} = \mu_q\frac{v_{dc}}{2} - e_{gq} \tag{10}$$

The averaged model of the DC/AC converter in the dq0 basis is given by the following equations:

$$L_2\frac{dx_7}{dt} + r_2 x_7 - L_2\omega x_8 = \mu_d\frac{x_9}{2} - x_{10} \tag{11}$$

$$L_2\frac{dx_8}{dt} + r_2 x_8 + L_2\omega x_7 = \mu_q\frac{x_9}{2} - x_{11} \tag{12}$$

with $(x_7, x_8, x_9, x_{10}, x_{11}) = (< i_{gd} >, < i_{gq} >, < v_{dc} >, < e_{gd} >, < e_{gq} >)$.

3 CONTROLLER DESIGN

3.1 Control Objectives

Control design is an essential task for stabilizing the operation of our system and achieving multiple objectives:

- Maximum Power Point Tracking Objective: The power delivered by photovoltaic panels depends on irradiance, temperature, and the voltage applied at the panel output. To ensure that the panels operate at the Maximum Power Point (MPP), an algorithm is required to determine the reference voltage v_{pv}^* corresponding to the MPP, as well as a command that controls the DC-DC converter to apply this voltage v_{pv}^* to the panel output.
- DC/AC converter input voltage regulation: To ensure the proper functioning of the DC/AC converter, its input voltage must be maintained stable at a predefined value. Thus, the regulation of the DC bus voltage is a necessary objective to ensure the stability of our system.
- Power Factor Correction Objective:Ensure a unity power factor in the electrical grid.

3.2 Maximum Power Point Tracking control

To ensure that the system extracts the maximum available power from the photovoltaic panels, we used the perturbation and observation algorithm, which determines the reference voltage v_{pv}^* corresponding to the point of maximum power. Then we controlled the DC-DC converter input using backstepping with integral action, in order to track this reference voltage v_{pv}^*. So first, we define the candidate Lyapunov function:

$$V_{1j} = \frac{1}{2}\gamma_{1j}^2 + \frac{1}{2}\varepsilon_{1j}^2 \tag{13}$$

with:

$$\varepsilon_{1j} = x_{1j} - x_{1j}^* \tag{14}$$

$$\gamma_{1j} = \int_0^t x_{1j} - x_{1j}^* \, dt \tag{15}$$

The addition of the integral action cancels out the static error to ensure accurate tracking. The derivative of the Lyapunov function $V1j$ must be negative for the error ε_{1j} to converge to zero.

$$\dot{V}_{1j} = \varepsilon_{1j}(\gamma_{1j} + \dot{\varepsilon}_{1j}) = -k_1\varepsilon_{1j}^2 \tag{16}$$

From equation (4):

$$\dot{\varepsilon}_{1j} = \frac{1}{C_{pv}}(x_{3j} - x_{2j}) - \frac{dx_{1j}^*}{dt} \tag{17}$$

$$\gamma_{1j} + \frac{1}{C_{pv}}(x_{3j} - x_{2j}) - \frac{dx_{1j}^*}{dt} = -k_1\varepsilon_{1j} \tag{18}$$

We consider x_{2j} as a virtual control law; we obtain:

$$x_{2j}^* = x_{3j} + C_{pv}(k_1\varepsilon_{1j} + \gamma_{1j} - \frac{dx_{1j}^*}{dt}) \tag{19}$$

The second step of this control strategy consists in designing a control law so that the current x_{2j} follows its reference x_{2j}^*.

$$\varepsilon_{2j} = x_{2j} - x_{2j}^* \tag{20}$$

The second Lyapunov function is given by:

$$V_{2j} = V_{1j} + \frac{1}{2}\varepsilon_{2j}^2 \tag{21}$$

From equation (20), equation (17) is rewritten as follows:

$$\dot{\varepsilon}_{1j} = \frac{1}{C_{pv}}(x_{3j} - \varepsilon_{2j} - x_{2j}^*) - \frac{dx_{1j}^*}{dt} \tag{22}$$

Replacing the expression for $x_{2j}^*$from equation (19) in equation (22) gives :

$$\dot{\varepsilon}_{1j} = -\frac{1}{C_{pv}}\varepsilon_{2j} - k_1\varepsilon_{1j} - \gamma_{1j} \tag{23}$$

$$\dot{V}_{1j} = \varepsilon_{1j}(\gamma_{1j} + \dot{\varepsilon}_{1j}) = -\frac{1}{C_{pv}}\varepsilon_{1j}\varepsilon_{2j} - k_1\varepsilon_{1j}^2 \tag{24}$$

From equations (21) and (24), we obtain the expression for the derivative of the Lyapunov function V_{2j}, given by the following equation:

$$\dot{V}_{2j} = -k_1\varepsilon_{1j}^2 - \frac{1}{C_{pv}}\varepsilon_{1j}\varepsilon_{2j} + \varepsilon_{2j}\dot{\varepsilon}_{2j} \tag{25}$$

For the error ε_{2j} to converge to zero, the derivative of the Lyapunov function V_{2j} must be negative.

$$\dot{V}_{2j} = -k_1\varepsilon_{1j}^2 - k_2\varepsilon_{2j}^2 \tag{26}$$

From equation (5), we have:

$$\dot{\varepsilon}_{2j} = \frac{1}{L_1}(x_{1j} - x_{5j}) + \frac{1}{L_1}u_j x_{5j} - \frac{r_1}{L_1}x_{2j} - \dot{x}_{2j}^* \tag{27}$$

Thus, based on equations (25), (26), and (27), we finally obtain the expression of the control law u_j, which allows regulating the voltage V_{pvj}.

$$u_j = \frac{L_1}{x_{5j}}(-k_2\varepsilon_{2j} + \frac{1}{C_{pv}}\varepsilon_{1j} + \frac{1}{L_1}(x_{5j} - x_{1j}) + \frac{r_1}{L_1}x_{2j} + \dot{x_2}_j) \tag{28}$$

3.3 DC/AC converter input voltage regulation

The second control objective in our system is to regulate the DC bus voltage v_{dc}. From Fig. 1, the DC bus voltage v_{dc} is equal to the sum of the voltages v_{dc1} and v_{dc2}.

$$v_{dc} = v_{dc1} + v_{dc2}; \tag{29}$$

From equation (3), we have:

$$C_{dc}\frac{dv_{dc1}}{dt} = i_{d1} - i_{dc} \tag{30}$$

$$C_{dc}\frac{dv_{dc2}}{dt} = i_{d2} - i_{dc} \tag{31}$$

Thus

$$C_{dc}\frac{dv_{dc}}{dt} = i_{d1} + i_{d2} - 2i_{dc} \tag{32}$$

The voltage dynamic v_{dc} can be expressed as a function of power by multiplying equation (32) by v_{dc}.

$$C_{dc}v_{dc}\frac{dv_{dc}}{dt} = v_{dc}i_{d1} + v_{dc}i_{d2} - 2v_{dc}i_{dc} \tag{33}$$

The expressions of the active and reactive power injected into the electrical grid, in the dq0 reference frame, are given respectively by the following equations:

$$P_{AC} = e_{gd}i_{gd} + e_{gq}i_{gq} \tag{34}$$

$$Q_{AC} = e_{gq}i_{gd} - e_{gd}i_{gq} \tag{35}$$

In order to ensure decoupling between active and reactive power control, the igd and igq currents are synchronized with a PLL so that:

$$e_{gq} = 0 \tag{36}$$

If we assume that the power losses in the two-level VSC converter and in the L_2 inductors are negligible (see Fig. 1), then we can write that :

$$v_{dc} i_{dc} = e_{gd} i_{gd} \tag{37}$$

Equation (33) therefore becomes :

$$\frac{1}{2} C_{dc} \frac{d v_{dc}{}^2}{dt} = v_{dc} i_{d1} + v_{dc} i_{d2} - 2 e_{gd} i_{gd} \tag{38}$$

From equations (9) and (38), we conclude that it is possible to control the v_{dc} voltage using a nested controller composed of two cascaded loops: an internal loop based on Lyapunov stability to control the i_{gd} current, and an external loop using a PI controller to regulate the v_{dc} dc bus voltage.

3.3.1 Inner control loop

The role of the internal regulator is not only to control the i_{gd} current, but also to guarantee a unity power factor on the electrical grid. From equations (34), (35), and (36), we have:

$$P_{AC} = e_{gd} i_{gd} \tag{39}$$

$$Q_{AC} = -e_{gd} i_{gq} \tag{40}$$

For the power factor to be unity, the reactive power injected into the grid must be zero.

$$i_{gq}^* = 0; \tag{41}$$

In the inner loop, we will design a controller based on Lyapunov stability to regulate the currents i_{gd} and i_{gq}. First, we define the two error variables ε_d and ε_q, and we introduce the candidate Lyapunov functions V_d and V_q :

$$\varepsilon_d = L_2(x_7 - x_7^*) \tag{42}$$

$$\varepsilon_q = L_2(i_8 - i_8^*) \tag{43}$$

$$V_d = \frac{1}{2}\varepsilon_d^2 \tag{44}$$

$$V_q = \frac{1}{2}\varepsilon_q^2 \tag{45}$$

To ensure the stability of the errors ε_d and ε_q towards 0, the derivative of V_d and V_q must be negative:

$$\dot{V}_d = \varepsilon_d \dot{\varepsilon}_d = -k_3 \varepsilon_d^2 \tag{46}$$

$$\dot{V}_q = \varepsilon_q \dot{\varepsilon}_q = -k_3 \varepsilon_q^2 \tag{47}$$

with $k_3 > 0$.
From Equations (11) and (12), we derive the expressions for the error derivatives $\dot{\varepsilon_q}$ and $\dot{\varepsilon_q}$:

$$\dot{\varepsilon_d} = \mu_d \frac{x_9}{2} - x_{10} - r_2 x_7 + L_2 \omega x_8 - L_2 \frac{dx_7^*}{dt} \tag{48}$$

$$\dot{\varepsilon_q} = \mu_q \frac{x_9}{2} - x_{11} - r_2 x_8 + L_2 \omega x_7 - L_2 \frac{dx_8^*}{dt} \tag{49}$$

By substituting the expressions for the errors ε_d and ε_q as well as their derivatives $\dot{\varepsilon_d}$ and $\dot{\varepsilon_q}$ into Equations (46) and (47) we finally obtain the control law expressions μ_d and μ_q.

$$\mu_d = \frac{2}{x_9}(x_{10} + r_2 x_7 - L_2 \omega x_8 + L_2 \frac{dx_7^*}{dt} - k_2 L_2 (x_7 - x_7^*)) \tag{50}$$

$$\mu_q = \frac{2}{x_9}(x_{11} + r_2 x_8 + L_2 \omega x_8 + L_2 \frac{dx_8^*}{dt} - k_2 L_2 (x_8 - x_8^*)) \tag{51}$$

3.3.2 External control loop

In the outer loop, we control the v_{dc} voltage. The necessary condition for the operation of a nested controller is that the response time of the inner loop must be very small than that of the outer loop, which means we can assume that:

$$x_7 = x_7^* \tag{52}$$

$$x_8 = x_8^* \tag{53}$$

Therefore, Equation 38 for the dynamics of the v_{dc} voltage can be rewritten as:

$$\frac{1}{2}C_{dc}\frac{d{x_9}^2}{dt} = x_9x_{41} + x_9x_{42} - 2x_{10}x_7^* \tag{54}$$

Assuming that:

$$y = {x_9}^2 \tag{55}$$

$$u = x_9x_{41} + x_9x_{42} - 2x_{10}x_7^* \tag{56}$$

Therefore, the equation of system 54 can be expressed by the following open-loop transfer function:

$$\frac{Y(s)}{U(s)} = \frac{2}{C_{dc}s} \tag{57}$$

The PI controller's output setpoint as a function of y and its reference y^* is given by :

$$U(s) = k_p(Y^*(s) - Y^*(s)) + \frac{k_i}{s}(Y^*(s) - Y^*(s)) \tag{58}$$

From Equations 57 and 58, the closed-loop transfer function of the system is obtained.

$$\frac{Y(s)}{Y(s)^*} = \frac{\frac{2k_p}{C_1}s + \frac{2k_i}{C_1}}{s^2 + \frac{2k_p}{C_1}s + \frac{2k_i}{C_1}} \tag{59}$$

We deduce the expression for the reference x_7^* as a function of the output u of the PI controller from Equation 56.

$$x_7^* = \frac{x_9(x_{41} + x_{42}) - u}{2x_{10}} \tag{60}$$

4 SIMULATION RESULTS

The objective of this section is to simulate the proposed system under different simulation scenarios, both under normal and severe operating conditions, in order to assess its performance. This system consists of two photovoltaic panels, each associated with a boost-type DC/DC converter, enabling the active power generated by these panels to be supplied to the DC/AC converter for injection into an AC power grid (see Fig. 1.). We performed the simulation in the Simulink environment using the parameters presented in table 1.

To evaluate the performance of our system, we tested it under different simulation scenarios. Between 0 and 0.5 seconds, both panels operate under normal conditions, meaning they receive the same irradiation of 1000 W/m² at a temperature of 25°C. Between 0.5 and 1 second, one of the panels is assumed to receive less intense irradiation than the other. in other words, it is partially shaded by an object that prevents it from capturing all the available

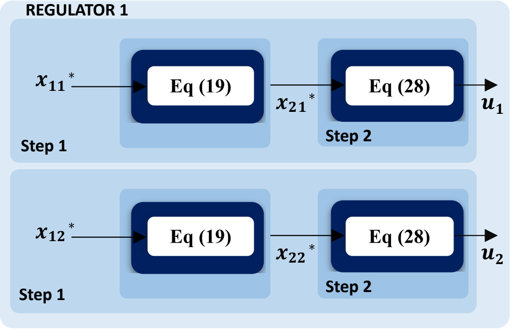

Figure 2. DC/DC regulator structure.

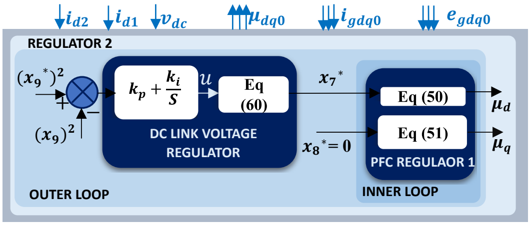

Figure 3. DC/AC regulator structure.

Table 1. SYSTEM PARAMETERS

Symbols	*Values*	*Symbols*	*Values*
C_{dc}	$50F$	E_g	$220V$
L_1	$3mH$	ω	$2\pi 50$
r_1	0.5Ω	L_2	$35mH$
C_{pv}	$0.2mF$	r_2	0.36Ω

sunlight. This allows us to observe the effect of this irradiation imbalance on the system's performance. Next, the system returns to a condition where both panels receive the same irradiation, to check whether the system returns to a behavior similar to that observed during the first period (between 0 and 0.5 seconds). Finally, between 2 and 2.5 seconds, it is assumed that one of the panels ceases to operate. The aim is to observe whether the other panel continues to operate normally, or if the failure of one panel affects the overall behavior of the system. At time 1.5, the temperature rises from 25 to 35 degrees. The following figures show the results of this simulation. Figs. 4 and 5 show that the v_{pv1} and v_{pv2} voltages follow their $v_{pv1}*$ and $v_{pv2}*$ references respectively, associated with the maximum power point (MPP), with satisfactory accuracy in the various simulation scenarios studied. This confirms that the first control objective, to ensure optimal tracking of the photovoltaic system's operating point in order to maximize the power extracted during variations in temperature and irradiance, has been successfully validated. Fig. 6 shows that the DC bus voltage is maintained stable at the reference value, and that the DC bus voltage regulator is capable of rejecting disturbances caused by variations in the power generated by the photovoltaic panels during

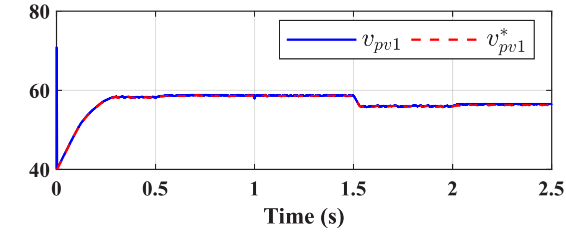

Figure 4. The regulation of the v_{pv1} voltage

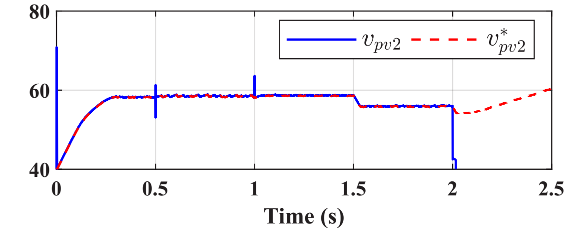

Figure 5. The regulation of the v_{pv2} voltage

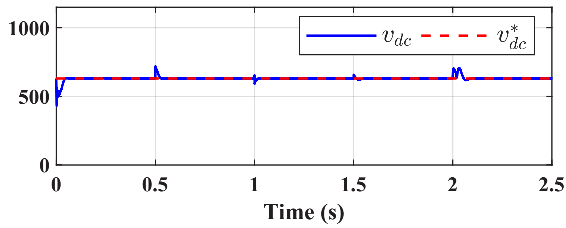

Figure 6. The regulation of the DC line voltage

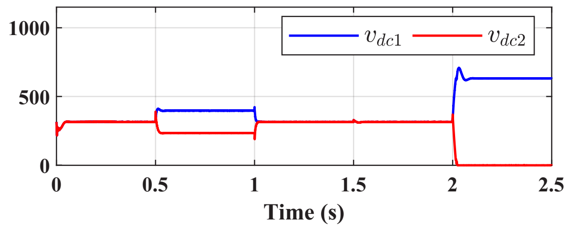

Figure 7. The evolution of the v_{DC1} and v_{DC2} voltages

changes in climatic conditions. Figs. 8 and 9 show that current igd follows its reference with good accuracy, and that current igq is maintained at zero. Since egd is a constant, we can deduce from equations (39) and (40) that variations in igd and igq represent variations in active and reactive power respectively. Thus, from Figs. 8 and 9,we can conclude that the internal V_{dc} voltage regulation loop controls the i_{gd} current with good accuracy, while maintaining a power factor equal to 1. Moreover, variations in the i_{gd} current do not disturb

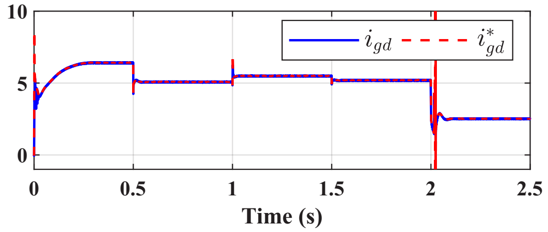

Figure 8. The evolution of i_{gd} current and its reference

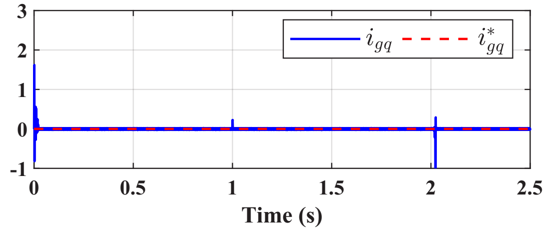

Figure 9. The evolution of i_{gq} current and its reference

the i_{gq} current, which means that our controller guarantees independent control of active and reactive power. We can therefore conclude that all our control objectives defined in Section 3 have been achieved. The configuration of our system consists of two DC/DC converters and a single DC/AC converter. In this architecture, each converter must be controlled to regulate the voltage at its input. The two DC/DC converters respectively regulate the voltages v_{pv1} and v_{pv2}, while the DC/AC converter controls the sum of the two v_{dc1} and v_{dc2}. Therefore, it is not possible to control v_{dc1} and v_{dc2} independently. Fig. 7 shows the variations of the voltages v_{dc1} and v_{dc2} over time. During the first period, between 0 and 0.5 s, v_{dc1} is equal to v_{dc2}. This is obvious, since both panels operate under identical conditions, meaning they generate the same power. In the following period, the voltage v_{dc1} becomes higher than v_{dc2} when panel 1 receives more intense irradiation than panel 2. Then, when both panels receive the same irradiation again, the voltages v_{dc1} and v_{dc2} also stabilize at the same value, corresponding to $\frac{v_{dc}}{2}$.

5 CONCLUSION

In this work, we have controlled a system composed of two DC/DC converters and a single DC/AC converter. The advantage of this topology is that it reduces the power flow through the DC/DC converters, which limits their heating and prevents them from reaching very high temperatures. The simulation results, obtained under different scenarios, show that the system remains stable even under critical operating conditions.

References

1. S. B. Kjaer, J. K. Pedersen and F. Blaabjerg, "A review of single-phase grid-connected inverters for photovoltaic modules," in IEEE Transactions on Industry Applications, vol. 41, no. 5, pp. 1292-1306, Sept.-Oct. 2005, doi: 10.1109/TIA.2005.853371.

2. Meghraj Morey, Nitin Gupta, Man Mohan Garg, Ajay Kumar, A comprehensive review of grid-connected solar photovoltaic system: Architecture, control, and ancillary services, Renewable Energy Focus, Volume 45, 2023, Pages 307-330, ISSN 1755-0084, https://doi.org/10.1016/j.ref.2023.04.009.
3. Kamran Zeb, Waqar Uddin, Muhammad Adil Khan, Zunaib Ali, Muhammad Umair Ali, Nicholas Christofides, H.J. Kim, A comprehensive review on inverter topologies and control strategies for grid connected photovoltaic system, Renewable and Sustainable Energy Reviews, Volume 94, 2018, Pages 1120-1141, ISSN 1364-0321, https://doi.org/10.1016/j.rser.2018.06.053.
4. Raghavendra, K. V. G Zeb, Kamran Muthusamy, Anand Krishna, T.N.V. Kumar, S Kim, Do-Hyun Kim, Minsoo Cho, Hwan-Gue Kim, Hee-Je. (2019). A Comprehensive Review of DC-DC Converter Topologies and Modulation Strategies with Recent Advances in Solar Photovoltaic Systems. Electronics. 9. 1-41. 10.3390/electronics9010031.
5. Valeria Boscaino, Vito Ditta, Giuseppe Marsala, Nicola Panzavecchia, Giovanni Tinè, Valentina Cosentino, Antonio Cataliotti, Dario Di Cara, Grid-connected photovoltaic inverters: Grid codes, topologies and control techniques, Renewable and Sustainable Energy Reviews, Volume 189, Part A, 2024, 113903, ISSN 1364-0321, https://doi.org/10.1016/j.rser.2023.113903.
6. Hammami, Manel Ricco, Mattia Ruderman, Alex Grandi, Gabriele. (2019). Three-Phase Three-Level Flying Capacitor PV Generation System with an Embedded Ripple Correlation Control MPPT Algorithm. Electronics. 8. 118. 10.3390/electronics8020118.
7. Barros, J. Rocha, Luis Silva, J.. (2023). Backstepping Control of NPC Multilevel Converter Interfacing AC and DC Microgrids. Energies. 16. 5515. 10.3390/en16145515.
8. Jyoti Sastry, Panagiotis Bakas, Hongrae Kim, Lei Wang, Antonios Marinopoulos, Evaluation of cascaded H-bridge inverter for utility-scale photovoltaic systems, Renewable Energy, Volume 69, 2014, Pages 208-218, ISSN 0960-1481, https://doi.org/10.1016/j.renene.2014.03.049.